IEEE Access
Multidisciplinary | Rapid Review | Open Access Journal

Received July 7, 2020, accepted August 30, 2020, date of publication September 7, 2020, date of current version September 22, 2020.

Digital Object Identifier 10.1109/ACCESS.2020.3022433

Assessing LoRa for Satellite-to-Earth Communications Considering the Impact of Ionospheric Scintillation

LARA FERNANDEZ[1,2,3], (Student Member, IEEE), JOAN ADRIA RUIZ-DE-AZUA[1,2,3], (Member, IEEE), ANNA CALVERAS[2], AND ADRIANO CAMPS[1,3], (Fellow, IEEE)

[1]CommSensLab-UPC, Department of Signal Theory and Communications, UPC BarcelonaTech, 08034 Barcelona, Spain
[2]Department of Network Engineering, UPC BarcelonaTech, 08034 Barcelona, Spain
[3]Institut d'Estudis Espacials de Catalunya (IEEC) - CTE-UPC, 08034 Barcelona, Spain

Corresponding author: Lara Fernandez (lara.fernandez.c@upc.edu)

This work was supported in part by the Spanish Ministry of Economy and Competitiveness, by the Spanish Ministry of Science, Innovation and Universities, Sensing with Pioneering Opportunistic Techniques, under Grant RTI2018-099008-B-C21, in part by the Unidad de Excelencia Maria de Maeztu under Grant MDM-2016-0600, in part by the European Regional Development Fund (ERDF) and the Spanish Government under Project PID2019-106808RA-I00 AEI/FEDER UE, and in part by the Secretaria d'Universitats i Recerca del Departament d'Empresa i Coneixement de la Generalitat de Catalunya under Grant 2017 SGR 376 and Grant 2017 SGR 219.

ABSTRACT Since the appearance of 5G, Internet of Things (IoT) has gained an increased interest, with multiple technologies emerging and converging to cover different user needs. One of the biggest challenges today is to have global IoT coverage, ensuring seamless communication with IoT devices placed in rural and even remote areas. Satellite constellations, and in particular CubeSats orbiting in Low Earth Orbit, can provide a solution to these challenges. Out of the technologies available, LoRa (Long Range) has a great potential for implementation in space-to-Earth satellite communications. As the space-to-Earth channel is different with respect to the conventional Earth-to-Earth one, it is important to asses the capabilities of LoRa in this new environment. This paper presents a study of different LoRa device configurations to identify the constrains for each one and determine which one is better for particular mission requirements. Also, the effect of ionospheric scintillation is assessed with a SDR-based (Software-Defined Radio) test set-up that evaluates the performance of this technology against with Humprey's ionospheric scintillation model. This phenomena produces deep signal intensity fadings and phase fluctuations in equatorial regions, and mainly phase fluctuations in high latitudes. The obtained metrics are the received power and the packet delivery ratio as a function of the intensity scintillation index, and show the robustness of the LoRa modulation in these new environments.

INDEX TERMS CubeSat, Internet of Things, ionospheric scintillation, LoRa, satellite communications.

I. INTRODUCTION

Internet of Things (IoT) aims at connecting devices (or ''things'') placed around the globe for environmental monitoring, safety purposes, amongst others. One challenge is that the amount of information of these devices must be exchanged around the world. Therefore, the ''things'' require the capability to transmit and receive information, and require connectivity to a network such as the Internet or other private networks. In some use cases, these devices are located in rural or remote areas, so they are designed to be low-power to reduce the maintenance interaction. This allows to power them with batteries, solar panels or by harvesting energy from the environment, achieving up to several years of autonomy. However, this low-power profile also constrains the transmitted power to communicate, impacting directly to the communications range and data rate.

Considering these premises, several IoT technologies have emerged covering different needs. Standards such as IEEE 802.15.4 [1], Bluetooth Low Energy (BLE) [2] or ZigBee [3]

The associate editor coordinating the review of this manuscript and approving it for publication was Pietro Savazzi.

define protocol stacks for devices that are low power and ideal for scenarios that require a short communications range, such as those in urban areas. On the contrary, if these devices are meant to be placed in rural or remote areas the deployment of a costly infrastructure would be necessary to connect them to a network.

Longer range IoT technologies have also appeared to ease the deployment of these devices in rural areas. Some of them are categorized as Low Power Wide Area Networks (LPWAN). LPWAN networks cover between 1 km and 10 km in urban areas, and between 10 km and 20 km in rural areas [4]. Each of the devices communicates independently with a gateway or base station which is connected to the network, as seen in Fig. 1. The communication is bidirectional, defining the uplink as the messages sent from the devices to the gateway and the downlink as the messages from the gateway to the devices. Having the gateway as the central node and the long communications range, reduces the infrastructure deployment in rural areas, and although this architecture is feasible to deploy in rural areas, in remote areas, such as the poles or oceans, it proves to be challenging and expensive. Thus, an alternative infrastructure that provides coverage to those remote areas is still necessary to deploy.

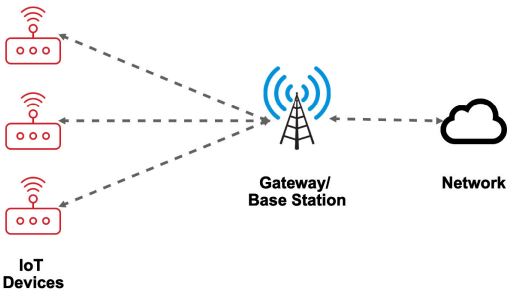

FIGURE 1. LPWAN technologies network architecture.

A constellation of Low Earth Orbit (LEO) Satellites can be a valid solution for these scenarios, as suggested in [5]. This constellation can provide global coverage, and lower latency and losses, as compared to Geostationary satellites which do not cover the poles and have more propagation delay and path losses. Moreover, in recent years a rapid development of technologies for small satellites has appeared, specially since the emergence of the CubeSat standard [6] which has boosted the technology development and reduced the launch costs. This standard defines the external envelope of the spacecraft, easing the interface with the launcher and allowing to perform a massive production of all the basic avionics included in the spacecrafts.

Taking these premises, a constellation of CubeSats that embark LPWAN gateways would provide coverage for those IoT devices placed in remote areas with a reasonable cost. However, space-to-Earth communications are more challenging than Earth-to-Earth ones, mainly because the channel losses and the Doppler frequency shifts are higher and -possibly- because of the ionospheric effects.

Losses are modeled with the Free Space Path Losses (FSPL) model, since line-of-sight between the Satellite and the Ground receiver is achieved. Additionally, the signals can also be attenuated by effects, such as atmospheric absorption, rain and cloud attenuation, and ionospheric scintillation. This last phenomena can play a critical role at UHF and L-bands [7], since it may produce deep and long intensity fadings and phase shifts, mainly in Polar and Equatorial regions. Moreover, due to the satellite dynamics there is a high Doppler frequency shift in the signal carrier. For all these reasons, it is necessary to asses the feasibility of embarking LPWAN technologies in satellites.

This work aims at presenting a trade-off study of different LPWAN technologies to be embarked in CubeSat platforms. In this trade-off the selected technology is LoRa. This technology has previously flown in two missions, one from Lacuna Space [8] and another one from Fossa Systems [9], and it has also been studied in [10]–[12] assessing different aspects of the technology if it was embarked in satellites. Overall, this work presents 1) a trade-off and analysis between the most relevant LPWAN technologies, 2) a link budget study to characterize the requirements of the system, and 3) the results of different tests which include the ionospheric effects.

The article is organized as follows: Section II presents the trade-off between different LPWAN technologies. Section III compares the link budget for different configurations of the LoRa system. Section IV details the results from the Ionospheric Scintillation tests. Finally, Section V presents the conclusions.

II. LPWAN TECHNOLOGIES TRADE-OFF

The LPWAN technologies to highlight currently used are Sigfox [13], NarrowBand-IoT (NB-IoT) [14], and LoRa [15]. To evaluate the different technologies a comparison of the Physical/Media Access Control (PHY/MAC) layer characteristics, such as modulation-coding techniques, frequency band, among others are considered to be used in LEO space-to-Earth communications.

Sigfox technology intends to connect objects to the digital world. This technology employs a Binary Phase Shift Keying (BPSK) modulation transmitting in unlicensed Industrial, Scientific, and Medical radio (ISM) bands. In some of these bands the transmitted power can be up to 22 dBm, and due to the modulation used the received power sensitivity is -126 dBm. This technology can achieve a data rate from 100 up to 600 bps, depending on the area, and it is capable to compensate a frequency drift up to ± 30 Hz [16]. Also, the MAC layer protocol is tolerant to the delay experienced when communicating using LEO satellites. However, the deployment of base stations is entitled solely to Sigfox, so it is not possible for third parties to embark gateways in satellites.

TABLE 1. Main LPWAN technologies comparison.

	Sigfox	NB-IoT	LoRa
Bandwidth (kHz)	0.1	200	125, 250, 500
Modulation	BPSK	QPSK	CSS
Frequency Band (MHz)	ISM	LTE	ISM
P_r (dBm)	22	23	22
P_s (dBm)	-126	-125	-125
Maximum data rate (kbps)	0,1 - 0,6	250	27
Delay Torelant	Yes	No	Yes
Network Interconnection Device	Sigfox Base Station	LTE Base Station	LoRa Gateway

NB-IoT, referred to as the cellular LPWAN, has been developed by the 3rd Generation Partnership Project (3GPP) [14] and is integrated as part of the 4G and 5G networks. This technology uses a narrow-band Quadrature Phase-Shift Keying (QPSK) modulation in a licensed band, with a maximum transmitted power of 23 dBm and a sensitivity of −125 dBm. The data rate is 26 kbps from the base station to the devices and 66 kbps from the devices to the base station, but eventually it can have peaks of up to 250 kbps. The NB-IoT waveforms and PHY/MAC layer protocol is impacted both by delay and Doppler [17]. Thus, this protocol needs to be adapted if it had to be used in space-to-Earth communications [18]. Moreover, the base stations are deployed by Mobile Network Operators (MNO).

LoRa is a technology developed by Semtech. It uses a proprietary Chirp Spread Spectrum (CSS) modulation, which is more resilient than others to interference and jamming, and it transmits in the unlicensed ISM bands. The LoRa technology has several parameters that must be configured in the transceivers, such as the transmitted power, Bandwidth (BW), Spreading Factor (SF), and Coding Rate (CR). The transmitted power can be up to 22 dBm, and the sensitivity can be as low as −125 dBm, offering a data rate up to 27 kbps. LoRa can be used with different MAC layer protocol, being LoRaWAN the most established one. LoRaWAN is open source and it is optimized for battery powered end-devices. There are several manufacturers that offer both LoRa modules and Gateways as COTS components. Therefore, it is feasible to propose a satellite gateway solution based on the LoRa technology.

Over the past years, LoRa has gained interest for satellite communications, assessing the limitations of the technology and even bringing it to space. For instance, an stratospheric balloon test [19] with LoRa modules was conducted to determine the maximum distance that could be achieved, reaching 832 km. Also, Lacuna Space [8] plans to launch a constellation of satellites with LoRa technology to provide global coverage. In fact, it has recently launched a CubeSat with a LoRa Gateway [20]. Also, Fossa Systems [9] has launched a PocketQube [21] with a LoRa transceiver, that can communicate with their Ground Module [22].

Some research has also been done on the topic. Authors in [10] analyse the compatibility of LoRaWAN with satellite communications, and identify the challenges in terms of MAC layer when deploying a LPWAN satellite backhaul. Also, in [11] the adaptability of the LoRa modulation for satellite communications is studied. Moreover, Authors in [12] have demonstrated that the LoRa modulation is able to compensate the Doppler effect experienced by LEO satellites. However, to authors' knowledge there is no physical layer study assessing the feasibility to use LoRa for LEO-based communications.

Given the compatibility of the LoRa modulation with satellite communications, and the ease to deploy gateways, as compared to NB-IoT and Sigfox, this is the technology that will be studied in this work.

III. ANALYSIS OF LINK BUDGET

This section aims at characterizing the LoRa technology physical layer in the space-to-Earth communications environment. The objective is to identify the requirements to have link budget between a CubeSat and a COTS ground device, and at the same time proposing a transceiver architecture for the spacecraft. The analysis is conducted for modules operating at 868 MHz and 915 MHz, because the 868 MHz band can be used over Europe, Russia and India, and the 915 MHz band over the United States of America and Australia.

A. SCENARIO

The link budget assesses the communications link between a satellite and a static ground terminal. The study considers different configurations for the satellite terminal, obtaining the expected received power and Signal-to-Noise ratio (SNR) for the uplink and for the downlink. The received power is compared to the sensitivity for each SF. Moreover, channel capacity is also taken into consideration, since having a larger capacity implies having more users that can access the network.

To perform the analysis there are some key aspects that have to be defined 1) the satellite orbit, which determines the distance between the satellite and the ground terminal; 2) the satellite and ground terminal configuration; 3) the channel model; and 4) the expected noise power.

1) SATELLITE ORBIT

The analysis considers that the satellite is orbiting in LEO with a circular orbit (i.e. eccentricity of 0°) at an altitude (h) of 550 km. The inclination of the orbital plane is not taken into consideration, since the distance between the satellite and the ground device is the same for any inclination.

Considering the orbit defined, a set of link budgets are computed according to different distances between the satellite and the ground device, which corresponds to different elevation angles of visibility with respect to the ground device. Thus, the maximum link distance would be 1815 km at an elevation of 10° and the minimum would be the orbital height 550 km, at an elevation of 90°.

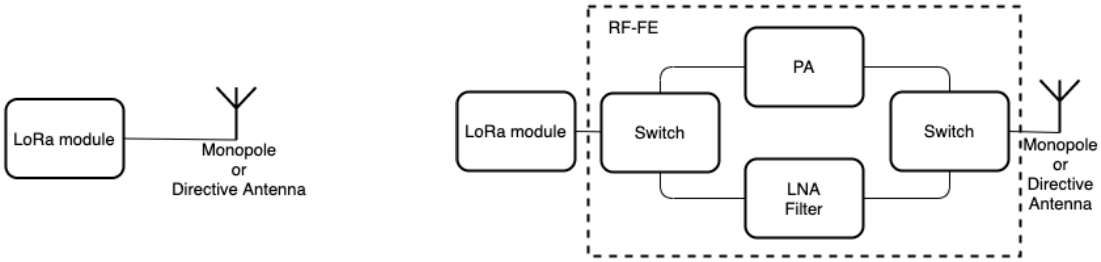

(a) MON and DIR configurations

(b) MON+RF-FE and DIR+RF-FE configurations

FIGURE 2. Satellite configurations.

The maximum Doppler frequency shift depends on the satellite speed, which is $v_{sat} = 7.8\ km/s$. Being the maximum experienced Doppler:

$$\Delta f = 22.56\ kHz \text{ for } f_0 = 868\ MHz \text{ and} \quad (1)$$
$$\Delta f = 23.78\ kHz \text{ for } f_0 = 915\ MHz. \quad (2)$$

2) SATELLITE AND GROUND TERMINAL CONFIGURATIONS

The satellite and the ground terminals are considered to have the same devices: the Semtech SX1261 module [23], for the 868 MHz band, and the SX1262 one [23], for the 915 MHz band. As mentioned before, the analysis considers four different satellite configurations. These have been selected to increase the transmitted power, receiving gain and the directivity of the antenna, to have link budget in the longer ranges experienced in satellite communications. The first configuration assumes that the satellite embarks a LoRa transceiver with a monopole antenna, (Fig. 2a). This configuration will be referred as MON.

The second configuration extends the former one with a radiofrequency Front End (RF-FE), which is conformed by a power amplifier (PA) in the transmitting chain, and a low noise amplifier (LNA) and a filter in the receiving chain, (Fig. 2b). The configuration will be referred as MON+RF-FE.

The third configuration consists of the LoRa transceiver with a directive antenna instead of a monopole, (Fig. 2a). This one will be referred as DIR. Finally, a combination of the front end and the directive antenna is done for the fourth configuration, (Fig. 2b), which will be called RF-FE+DIR.

The ground terminal is assumed to have the first configuration (MON) with the LoRa module and monopole antenna, to simplify it and prevent having to point the antennas towards the spacecraft which would be necessary if using a directive antenna. Thus, the transmission power and modulation parameters are assumed to be the same for the MON configuration and for the ground terminals.

The transmitted power is configured to 14 dBm at 868 MHz and 22 dBm at 915 MHz, these values are the maximum ones according to the datasheet of the modules [23]. However, for the configurations that incorporate the RF-FE, the transmitted power is the one given by the PA, 30 dBm [24] and in the receiving chain the LNA is considered to have a gain of 16 dB [25].

The gain of the antennas is considered to be 0 dB for the monopole and 10 dB with the directive antenna. For this directive antenna the directivity could be achieved for example, with a 3 element patch antenna array, a 4-5 turns helix antenna, or a 4-5 elements Yagi-Uda antenna.

In the LoRa modulation the BW is configurable, and according to the datasheet [23], this parameter determines the maximum shift in the central frequency that the modules are able to compensate, and the noise power. The shift that the modules compensate can be up to 25% of the BW. This value has to be higher than the Doppler effect, in order to be naturally compensated by the module itself. However, this confronts with the relationship between the bandwidth and the noise power. Specifically, the bandwidth should be the smallest value possible to reduce the noise power and transmission time. Considering that the typical values are 125 kHz, 250 kHz and 500 kHz, and taking into consideration the two constrains mentioned above the optimum BW would be 125 kHz, since it can compensate up to ± 31.25 kHz of frequency shift.

The CR is also configurable, and can be set to 4/5, 4/6, 4/7 or 4/8, having 1, 2, 3 or 4 bytes of redundancy respectively, it should be noted that the CR is defined as the number of information bits divided by the total number of bits sent. This CR provides a code gain that for the LoRa modulation is

TABLE 2. Summary of satellite configurations.

Configuration	LoRa Module	RF-FE	Monopole Ant.	Directive Ant.	Parameters
MON	X		X		$P_t = 14/22$ dBm $G_{LNA} = 0$ dB $G_{ANT} = 0$ dB
MON+RF-FE	X	X	X		$P_t = 30$ dBm $G_{LNA} = 16$ dB $G_{ANT} = 0$ dB
DIR	X			X	$P_t = 14/22$ dBm $G_{LNA} = 0$ dB $G_{ANT} = 10$ dB
DIR+RF-FE	X	X		X	$P_t = 30$ dBm $G_{LNA} = 16$ dB $G_{ANT} = 10$ dB

not specified, in fact, the sensitivity depends only on the SF and the BW. So, in the link budget no coding rate gain is considered, being a worst case scenario (i.e. conservative study).

All these modulation parameters determine the capacity (C) in bps of the channel, which is computed as shown in 3, where C is the capacity of the channel in bps, BW is the Bandwidth in Hz, SF is the selected SF and CR the used coding rate.

$$C = SF \frac{CR}{\left[\frac{2^{SF}}{BW}\right]} \tag{3}$$

As a consequence, the capacity increases with an increase of the BW and with a decrease of the SF. Also, the higher the redundancy the less C in the channel. For this reason, since the CR is not considered for the link budget, the best case in terms of capacity will be assumed, which corresponds to a CR of $\frac{4}{5}$, having the lowest redundancy possible.

Finally, a safety margin of 3 dB is added to the received power. This margin is included to compensate extra losses that may not be considered such as the accuracy of transmitted power of the transceivers, which according to the datasheet is ± 2 dB [23].

3) CHANNEL

The channel in space-to-Earth communications experiences free-space path losses (FSPL). These FSPL in dB can be calculated as a function of the frequency (f) in Hertz and the distance (d) in meters between the satellite and the ground terminal, as shown in (4).

$$FSPL = 20log(d) + 20log(f) - 147.55 \tag{4}$$

Aside from the losses introduced by FSPL, 3 dB of atmospheric losses, and 3 dB of polarization losses are also considered, which is the maximum for a link between a linear polarized antenna and a circular one. Moreover, 3 dB of pointing losses are taken into account for the configurations that include a directive antenna, but are considered negligible (i.e. 0 dB) when using a monopole.

4) NOISE POWER

To calculate the noise power, first the noise temperature has to be defined. The systems noise temperature is different for uplink, ground terminal to satellite, and downlink, satellite to ground terminal. In the uplink 290K are considered as a worst case [26], so this antenna temperature will be used for the analysis.

For the downlink the antenna temperature can be calculated as

$$T_A = T_{SKY} + T_{GROUND}, \tag{5}$$

where the T_{GROUND} can be estimated as 2320K for a median business area, whilst the T_{SKY} can be estimated as 20K. Thus, T_A equals to $2340K$.

Considering the noise temperatures, the expected noise power is:

$$N_{uplink} = -108 \text{ dBm and} \tag{6}$$

$$N_{downlink} = -114 \text{ dBm.} \tag{7}$$

B. LINK BUDGET RESULTS

The results for the link budget analysis are presented in this section, both for the 868 MHz modules and the 915 MHz ones.

1) LINK BUDGET AT 868 MHz

The results for the 868 MHz uplink and downlink are shown in Figs. 3 and 4, respectively. These plots represent the received power, P_r, and the Signal to Noise Ratio (SNR) as a function of the elevation of the satellite. The sensitivity, P_s, for each of the SFs is also represented, to asses for which values of SF is possible to have communication with the different configurations.

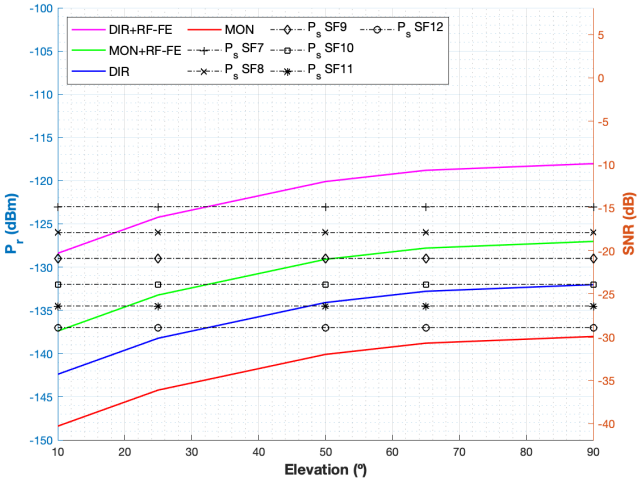

FIGURE 3. Uplink received power P_r and SNR for 868 MHz transceiver.

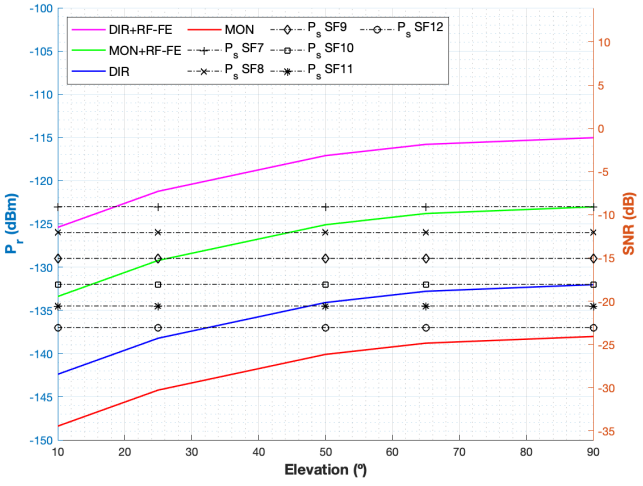

FIGURE 4. Downlink received power P_r and SNR for 868 MHz transceiver.

For the MON configuration (the red line in the plots) the communication cannot be established in any elevation. Therefore, this configuration is not suitable for space-to-Earth communications. In fact it is required to extend this architecture with other components.

If, instead the DIR configuration is considered, which corresponds to the blue line in the plots, the communication is possible from 33° of elevation with an SF of 12 and from 48° with an SF of 11, both for the uplink and the downlink. Although with a directive antenna is possible to have communication, placing this antenna in a satellite is more challenging than placing a monopole. Mainly because these antennas require pointing the spacecraft towards the surface of the Earth, so it is necessary to have precise attitude determination and control.

An alternative to directive antennas is to have the LoRa transceiver with an RF-FE and a monopole antenna, which corresponds to the MON+RF-FE configuration. This configuration, represented as a green line, is also better in terms of link budget with respect to the other two already presented, and it does not require precise attitude pointing. In the downlink it achieves communication for any elevation with an SF of 11 and from an elevation of 45° with an SF of 8, and in the uplink for any elevation with an SF of 12 and from 52° with an SF of 9.

Finally, the DIR+RF-FE configuration, shown as a pink line, is able to achieve communication in the downlink with an SF of 8 for any elevation, and with an SF of 7 for elevations above 19°. In the case of the uplink, communication is feasible for any elevation for an SF of 9, and with an SF of 7 from 32°. Even though this configuration faces the challenges of including the directive antenna, it is the one that provides more channel capacity since an SF of 7 can be used.

A summary with the minimum required elevation for each of the SF and configurations is shown in Table. 3. As a conclusion, having the MON configuration communication is not viable. A solution to improve the link budget could be either DIR or the MON+RF-FE configurations. Between these two solutions, the MON+RF-FE has more performance and is also less demanding in terms of attitude pointing.

TABLE 3. Minimum elevation to have communication in the uplink and the downlink for 868 MHz.

Configuration	Minimum elevation (°)					
	Spreading Factor					
	12	11	10	9	8	7
Uplink						
MON	-	-	-	-	-	-
DIR	33	48	-	-	-	-
MON+RF-FE	10	20	32	52	-	-
DIR+RF-FE	10	10	10	10	18	32
Downlink						
MON	-	-	-	-	-	-
DIR	33	48	-	-	-	-
MON+RF-FE	10	10	15	26	45	-
DIR+RF-FE	10	10	10	10	10	19

Finally, the DIR+RF-FE configuration could be an option for applications that require having a higher capacity or applications with a high density of users.

2) LINK BUDGET AT 915 MHz

The link budget with the 915 MHz presents larger received power than in the 868 MHz case, since the transmitted power is higher, as explained in Section III-A2. The results for this configuration can be seen in Figs. 5 and 6.

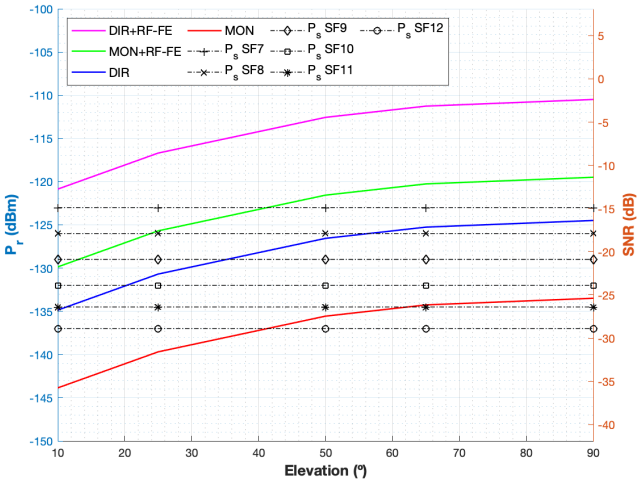

FIGURE 5. Uplink received power P_r and SNR for 915 MHz transceiver.

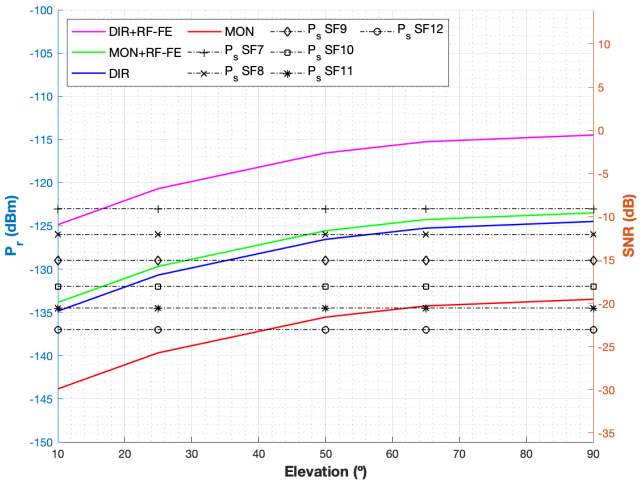

FIGURE 6. Downlink received power P_r and SNR for 915 MHz transceiver.

In this case the communications with the MON configuration is possible from an elevation of 42° at an SF of 12 and above 62° for an SF of 11. However, if the DIR one is used, communication is possible for any elevation with an SF of 11 and from 60° of elevation communication is feasible with an SF of 8.

The MON+RF-FE configuration has a similar received power in the downlink than the DIR configuration. However, for the uplink it can achieve communication at higher SFs,

having link budget for any elevation with an SF of 10 and from 42° with an SF of 7.

Finally, for the DIR+RF-FE communication is possible for any elevation at a SF of 7 for the uplink and from 17° for the downlink.

Table. 4 summarizes the minimum elevations required to have communication with the different configurations. Overall with the 915 MHz modules there is more margin in the link budget as compared to the 868 MHz ones, since the transmitted power is 8 dB higher. Thus, even with the MON configuration the communication is feasible, but only at high elevations and with low data rate. If more channel bandwidth is needed using either the DIR or MON+RF-FE configurations is an option. However, since the MON+RF-FE has higher received power and it does not require to have accurate pointing of the satellite, this option is preferred. Finally, having the configuration with both the RF-FE and a directive antenna allows using the maximum channel capacity that the LoRa modulation can provide with the fixed bandwidth.

TABLE 4. Minimum elevation to have communication in the uplink and the downlink for 915 MHz.

Minimum elevation (°)						
Configuration	Spreading Factor					
	12	11	10	9	8	7
Uplink						
MON	42	62	-	-	-	-
DIR	10	12	20	35	56	-
MON+RF-FE	10	10	10	13	24	42
DIR+RF-FE	10	10	10	10	10	10
Downlink						
MON	42	62	-	-	-	-
DIR	10	10	21	35	58	-
MON+RF-FE	10	10	16	30	48	-
DIR+RF-FE	10	10	10	10	10	17

IV. ANALYSIS OF IONOSPHERIC SCINTILLATION EFFECTS

This section presents the impact of the ionosphere scintillation in the propagation. This phenomena cannot be evaluated as part of the link budget, since it produces rapid fadings with variable durations. For that reason, a set of tests is performed to asses the impact that ionosphere scintillation has on the LoRa modulation.

A. THEORETICAL BACKGROUND

Ionospheric scintillation are rapid intensity and phase fluctuations induced in the radio-signals as they pass through the ionosphere. This phenomena is produced by the spatial inhomogeneities in the electron density in the ionosphere that produce a focusing/defocusing of the electromagnetic waves.

The parameter that models the effect of ionosphere intensity scintillation is the S_4 index which, as seen in 8, is calculated from the intensity of the signal (I). Regarding the phase, it is characterized by σ_ϕ. However, the implemented model for the tests, is the Humprey's model [27], that uses two parameters S_4 and τ_0, which is related to the fading

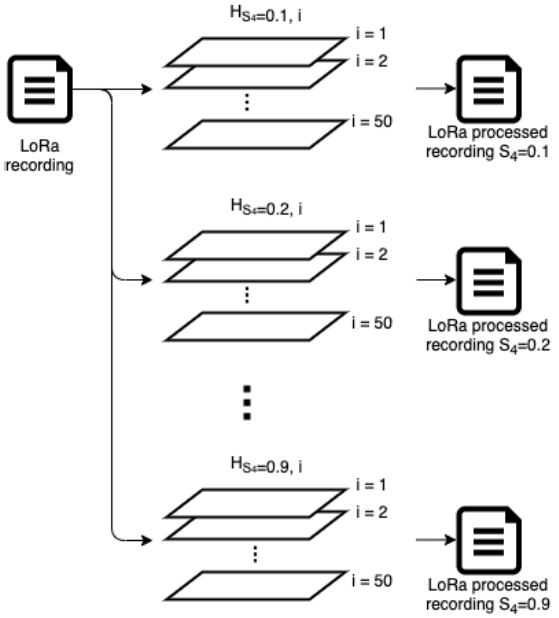

FIGURE 7. LoRa signal processing modelling.

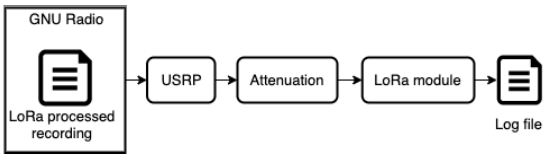

FIGURE 8. LoRa signal reproduction using GNU Radio and log file storing.

duration. The S_4 and τ_0 can be related to an S_4 and σ_ϕ pair.

$$S_4 = \sqrt{\frac{\langle I^2 \rangle - \langle I \rangle^2}{\langle I \rangle^2}} \tag{8}$$

The typical values of S_4 index range from 0.1 to 1, values below 0.3 are considered as low ionospheric scintillation, from 0.3 up to 0.6 it is medium, and from 0.7 upwards it is severe scintillation. These tests are performed for S_4 between 0.1 and 0.9. τ_0 is set to 0.4 s, which is a typical average value [27].

B. TEST SETUP

These tests are performed with the 915 MHz modules using the same bandwidth as in the link budget of 125 kHz with a SF of 7, since it is the option that provides a higher channel capacity. Moreover, the study is performed for two different CRs, $\frac{4}{5}$ and $\frac{4}{6}$, to asses the impact of having redundancy.

Taking into account these modulation parameters, communication is only possible for the RF-FE and Directive antenna configuration of the link budget. Out of this configuration the best and worse cases in terms of received power will be tested. The best case corresponds to the uplink with a received power of -110 dBm and the worst case is achieved in the downlink and corresponds to the sensitivity for this SF which is -123 dBm.

To perform the tests, a LoRa signal was recorded using an Ettus Universal Software Radio Peripheral (USRP) B200 mini. This recording contains LoRa packets which are sent periodically, with a periodicity higher than the transmission and processing time of the modules, ensuring that no packets are lost due to unavailability of the receiver. Also, the packets for both CR configurations have the same Payload length, which implies that adding redundancy enlarges the size of the packets.

One recording is done for each of the CR configurations and a total of 500M samples at a sampling frequency of 1 Msps are recorded for each one. The number of samples is constrained by the amount of data generated by the recordings and the post processing. It should be noted that number of samples of the recording, determines the total number of packets recorded, which are 68 packets for the CR of $\frac{4}{5}$ configuration and 55 packets for the CR of $\frac{4}{6}$.

These recorded signals are then processed by introducing Humprey's ionospheric scintillation model [27], [28] to simulate the propagation channel. The processing is done by multiplying the phase and quadrature components of the recorded LoRa signal with a realization of the channel model. This process is repeated 50 times and it is saved in a file for each of the S_4 indexes and for each of the CRs. This process is ilustrated in Fig. 7.

Overall, the resulting processed recordings contain 3300 packets for the CR of $\frac{4}{5}$ case, which corresponds to 50 realizations of the channel with 68 packets each, and 2850 packets for the CR of $\frac{4}{6}$ case, so 50 realizations of 55 packets each. Each of these files are reproduced twice, so that the results obtained are statistically representative.

The processed recordings are then reproduced, using GNURadio and the Ettus USRP B200 mini. Then, the signal is attenuated, so that the received power corresponds to the best and worst cases of the link budget, explained in Section III. Finally, the signal is received by a LoRa module. This module stores the packets received with the received power in a log file for post-processing as seen in Fig. 8. The packets stored in the log files are those that have been correctly received after demodulation, which means that packets that contain errors are discarded.

It should be noted that the metrics obtained refer to received power instead of the Received Signal Strength Indicator (RSSI), because spread spectrum modulations can be received below the noise level. This implies that when the received signal is below the noise level the RSSI measured corresponds to the noise power and the SNR is negative. These two metrics are sensed by the LoRa modules. Therefore, the received power in dBm is computed using the RSSI in dBm and the SNR in dB, as follows:

$$P_r = RSSI \text{ if } SNR \geq 0 \tag{9}$$

$$P_r = RSSI + SNR \text{ if } SNR < 0 \tag{10}$$

From the log files two different metrics are obtained: the Packet Delivery Ratio (PDR) for each of the blocks, which corresponds to the number of received packets with respect to the number of transmitted packets. This PDR is plotted using a statistical boxplot representation, as in [29]. Also, the number of packets received with a certain received power is plotted for different S_4 values. Finally, the throughput achieved for each of the cases is compared. This throughput is calculated as the division of the payload data contained in all the packets received correctly over the span of the total time.

C. RESULTS

The results for the best case configuration for a CR of $\frac{4}{5}$ are shown in Figs. 9a and 9b. With this configuration the PDR is 100 % for the four lowest values of scintillation index (i.e. S_4 from 0.1 to 0.4). This indicates that all the transmitted packets have been received and processed correctly. For higher values

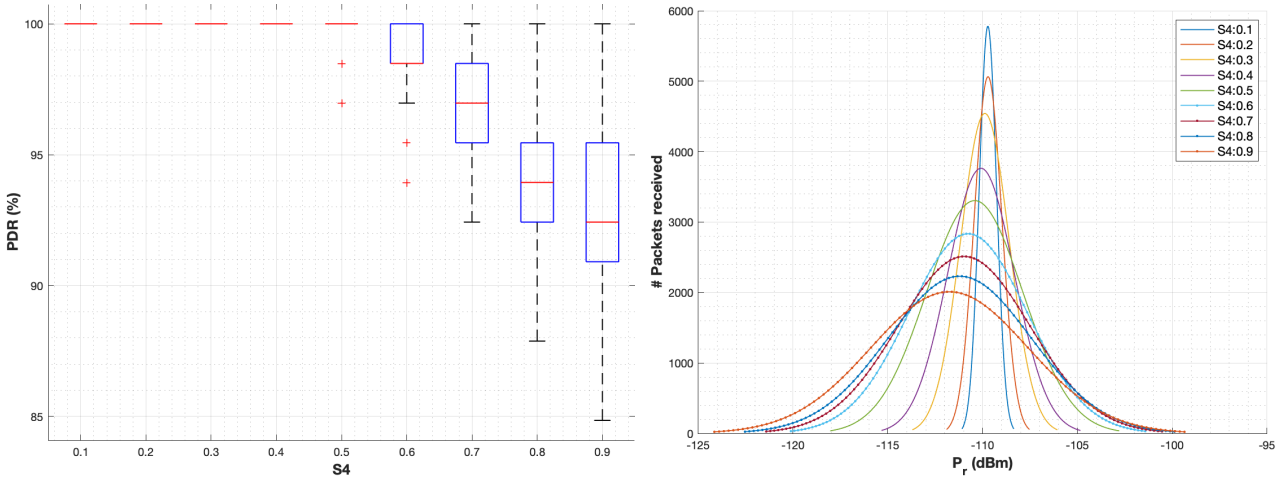

(a) PDR for the best case with $CR = \frac{4}{5}$

(b) Number of received packets for the best case with a $CR = \frac{4}{5}$

FIGURE 9. Measured results with experimental set-up for the best case with $CR = \frac{4}{5}$.

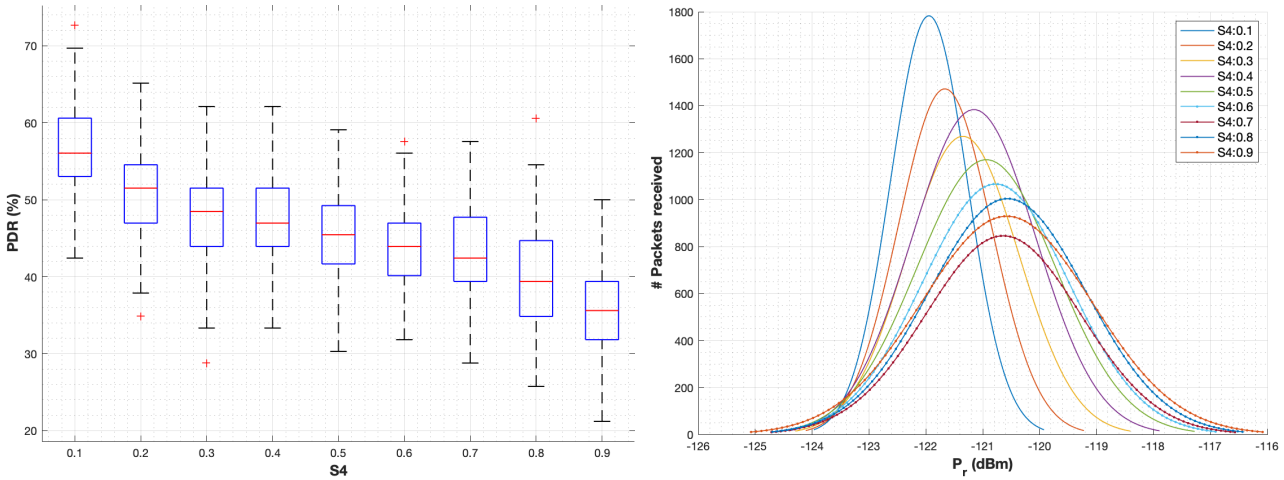

(a) PDR for the worst case with $CR = \frac{4}{5}$

(b) Number of received packets for the worst case with a $CR = \frac{4}{5}$

FIGURE 10. Measured results with experimental set-up for the worst case with $CR = \frac{4}{5}$.

of S_4 it decreases up to a 92 %. Given that this configuration has margin with respect to the sensitivity of the modules, most of the packets affected by fadings are still received and only those that are affected by multiple deep fadings are not received.

Regarding the mean received power, it has a trend to decrease as S_4 increases, which is caused by the fadings introduced by ionospheric scintillation. The variance of the received power increases with the scintillation index. As severity increases more fadings occur with different amplitudes, leading to different possible values of received power.

Having the same CR, but with the worst condition of received power, the PDR has the same tendency: it decreases as the severity increases, as seen in Fig. 10a. Although, due to the link conditions in this case the PDR is has a mean of 57% for the lowest scintillation decreasing up to 36 % for the severest S_4.

The received power for the worst case for a CR of $\frac{4}{5}$ is shown in Fig. 10b. In this case the mean received power is higher as severity increases. This is because the packets that are affected by fadings are lost, whilst those that either do not suffer fadings or are affected by the small gains that the channel can introduce are still received. Also, the variance in the received power is larger, as with the previous configuration.

For a CR of $\frac{4}{6}$ and in the best case, it can be seen in Fig. 11a, that the trend of PDR is the same as in the previous two cases, where the PDR decreases as iopnospheric scintillation severity increases. Also, comparing this case with the best case for a CR of $\frac{4}{5}$, some packets are not received even for

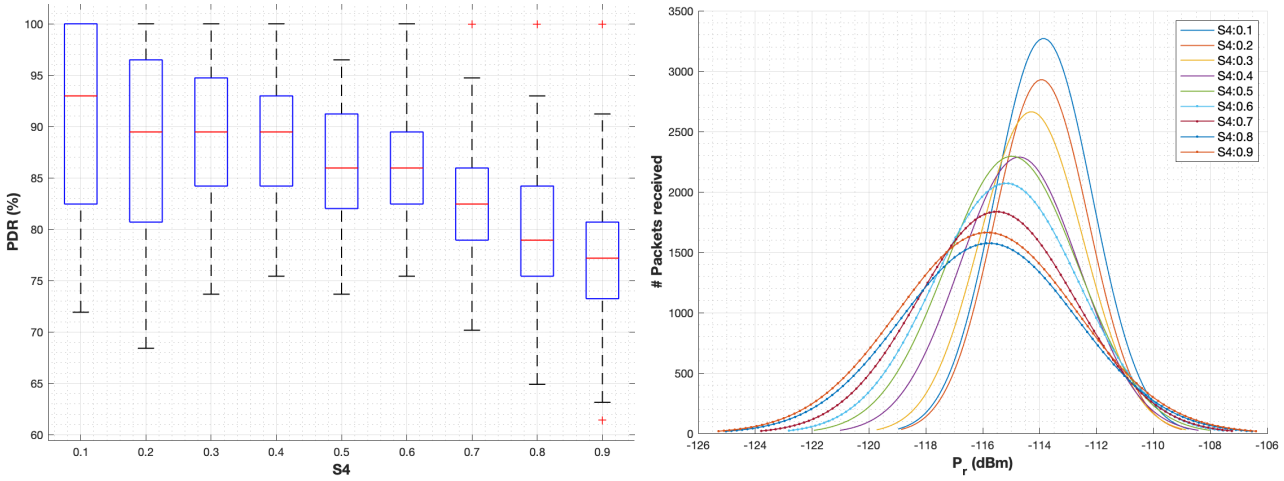

(a) PDR for the best case with $CR = \frac{4}{6}$

(b) Number of received packets for the best case with a $CR = \frac{4}{6}$

FIGURE 11. Measured results with experimental set-up for the best case with $CR = \frac{4}{6}$.

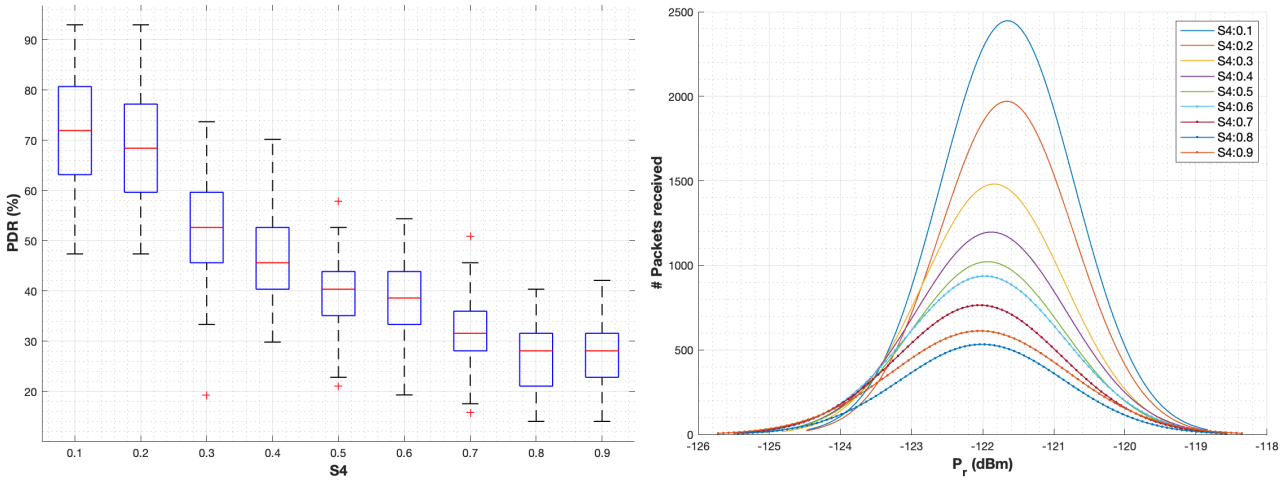

(a) PDR for the worst case with $CR = \frac{4}{6}$

(b) Number of received packets for the worst case with a $CR = \frac{4}{6}$

FIGURE 12. **Measured results with experimental set-up for the worst case with $CR = \frac{4}{6}$.**

the lowest values of severity. So, for $S_4 = 0.1$ 94% of the packets are received, decreasing up to 87% for the severest scintillation.

In terms of received power, as shown in Fig. 11b, the trend is also similar to the best case for a CR of $\frac{4}{5}$. So, overall the mean received power decreases and the variance increases as scintillation is more severe. However, in this case the variance for lower S_4 is higher compared to the best case with a CR of $\frac{4}{5}$. This can be caused by the CR, since having a CR implies having a coding gain that can vary from packet, having different values of received power.

For the worst case with a CR of $\frac{4}{6}$, as seen in Fig. 12a, the PDR also decreases with increasing Scintillation severity. However, comparing the PDR of both worst cases, it can be seen that with the additional redundancy the receiver is able to receive more packets for low severities. This indicates that when the link is in the limit of sensitivity the CR is able to correct some errors, allowing to receive some packets that would be lost with lower CR. However, if severity increases having more redundancy worsens the PDR.

Looking at the mean received power for the CR of $\frac{4}{6}$ case, Fig. 12b, it can be seen that it is the same for all values of Scintillation, with similar variance. Comparing these results with the worst case with a CR of $\frac{4}{5}$, it can be appreciated that not only the packets affected by the small gain of scintillation are received, but also some affected by fadings.

Fig. 13 represents the throughput for the four cases considered as part of these tests. It should be noted that the throughput has the tendency as the PDR, since it is computed based on the number of packets correctly received over a span of time. Overall, for all four cases the throughput decreases as the severity of ionospheric scintillation increases, meaning that the deep fadings experienced in the channel attenuate the signal of some packets below the sensitivity and these are no longer received.

Comparing the two best cases, it can be seen that the throughput is higher having less redundancy, CR of $\frac{4}{5}$ case. This means that, although the total amount of information sent is the same and the payload data (i.e. useful information) in each packet is also the same, less useful information is actually sent in the span of time. Indeed, this can be seen in the number of packets that were recorded for each of the cases, for a CR of $\frac{4}{5}$ there are 68 packets per recording whilst for a CR of $\frac{4}{6}$ there are 55. Moreover, since there is margin in the link budget, in most cases it is not necessary to detect and correct errors and redundancy does not have a positive impact on the throughput. In order to quantify the number of packets that are affected by strong fadings and that may require detection and correction of errors, the channel is further analysed.

In this case, as it can be seen in Fig. 9b, the packets are received with a mean received power of -110 dBm and the minimum value is -125 dBm, so an attenuation of 15 dB would be required to be certain that the packets are lost. For this reason, the duration of the fadings and the time between fadings which are deeper than 15 dB is calculated. As seen in Table. 5, the mean duration of the fadings is represented as μ_t and its standard deviation as σ_t, the mean time between fadings is represented as μ_b (ms) and the standard deviation as σ_b. Comparing the mean duration of the fadings and the time between fadings with the transmission time of the packets, which is $t_{tx} = 81.9$ ms for a CR of $\frac{4}{5}$ and $t_{tx} = 98.3$ ms for a CR of $\frac{4}{6}$, it can be seen that from an $S_4 = 0.4$ there is a high chance of having at least one fading within each packet. Moreover, from that value of S_4 there is a progressive decrease in the throughput in both CR configurations.

If the two worst cases of the CR configurations are compared, it is noticeable that by having more redundancy the throughput is higher for low values of S_4, although it is lower for higher values of S_4. This means that adding redundancy the CR is able to detect and correct errors, even if the packets

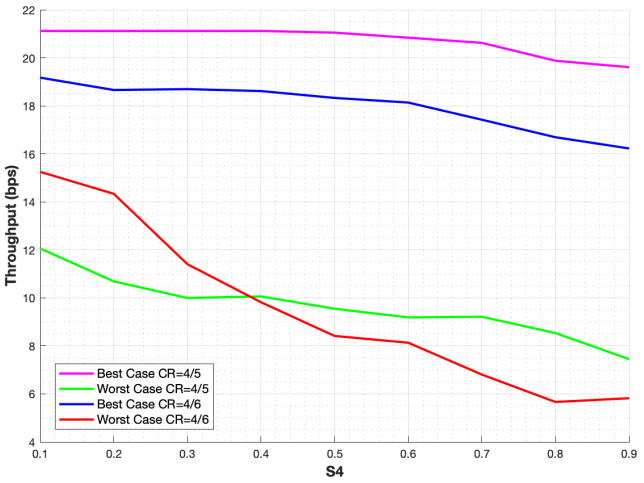

FIGURE 13. Throughput comparison for the worst cases of link budget.

TABLE 5. Duration and time between fadings below 15 dB for the S_4 cases.

S_4	μ_t (ms)	σ_t (ms)	μ_b (ms)	σ_b (ms)
0.1	6.3	6.8	307.4	250.8
0.2	3.1	3.5	151.3	122.7
0.3	2.1	2.4	102.8	83.3
0.4	1.7	1.9	80.4	65.1
0.5	1.5	1.6	67.5	57.4
0.6	1.4	1.4	57.0	52.2
0.7	1.3	1.3	48.7	49.0
0.8	1.3	1.5	41.7	46.0
0.9	1.2	1.3	37.0	43.9
μ_t: mean duration of fadings σ_t: standard deviation of fadings μ_b: mean time between fadings σ_b: standard deviation of time between fadings				

are affected by fadings. However, there is one point for more severe scintillation where the CR is no longer able to correct the errors within a packet. To have a better understanding on how the fadings are affecting the packets, it is also necessary to analyse the duration and frequency of these. In this case the attenuation necessary to not receive the packets is 4 dB, since the mean received power is -122 dBm and the minimum is -126 dBm, as seen on Fig. 12b. Thus, the fadings that have an attenuation lower than 4 dB will be considered.

The duration and time between fadings below 4 dB can be seen in Table. 6. Overall, the mean duration of the fadings and the time between fadings decreases with an increase in severity, although these are shorter. If the transmission time of the packets, which is $t_{tx} = 81.9$ ms for a CR of $\frac{4}{5}$ and $t_{tx} = 98.3$ ms for a CR of $\frac{4}{6}$, is compared with the fadings, it can be seen that for both configurations of CR in mean only one fading affects the packets up to an $S_4 = 0.4$ and for higher values in mean two or more fadings can affect the packets. If the throughput is correlated with the number of fadings, in the situation where in mean there is one fading per packet (i.e. S_4 up to 0.4), having more redundancy provides

TABLE 6. Duration and time between fadings below 4 dB for the S_4 cases.

S_4	μ_t (ms)	σ_t (ms)	μ_b (ms)	σ_b (ms)
0.1	64.7	55.5	312.4	198.6
0.2	32.2	29.6	153.6	100.3
0.3	21.1	19.9	99.2	67.9
0.4	15.8	15.5	70.6	51.2
0.5	12.9	15.7	54.1	42.1
0.6	11.0	18.1	43.4	34.8
0.7	10.0	22.4	35.9	29.6
0.8	9.2	25.6	30.1	25.3
0.9	8.4	25.7	25.3	21.8
μ_t: mean duration of fadings σ_t: standard deviation of fadings μ_b: mean time between fadings σ_b: standard deviation of time between fadings				

more throughput, because for a CR of $\frac{4}{6}$ more errors can be detected and corrected. Contrarily, for higher values of S_4 the packets contain too many errors, and the CR is no longer able to correct them. In fact, in this more severe scenario having a higher transmission time implies having a higher probability of being affected by fadings.

V. CONCLUSION AND FUTURE WORK

This study has evaluated the limitations of the LoRa technology when using it in space-to-Earth satellite communications. This is first done by means of a theoretical analysis, where the link budget is calculated considering the channel model in space-to-Earth communications. Then, a set of tests are performed to assess the robustness of the LoRa modulation when it is affected by ionospheric scintillation.

As part of the link budget study, four different configurations in terms of front end and antenna for the satellite are compared. The cases are: (1) having the LoRa module and a monopole antenna, (2) having the LoRa module and a directive antenna, (3) having a LoRa module with a radiofrequency front-end and a monopole antenna, and (4) having a LoRa module with the radiofrequency front-end and a directive antenna.

The analysis has been conducted for the 868 MHz and for the 915 MHz modules with a BW of 125 kHz, so that the modulation is able to compensate the maximum Doppler frequency shifts. The coding gain that the CR provides is not considered, since there is no open information on the gain that it provides. This analysis compares the received power and SNR as a function of elevation with the sensitivity power for each of the SFs. This is done both for the uplink and the downlink.

The results show that just having the MON configuration communication is not possible throughout the whole orbit for any spreading factor for the 868 MHz modules, and it is only possible for high elevations, and an SF of 12 for the 915 MHz one. Thus, adding a RF-FE or a directive antenna is required.

Between having the DIR and the MON+RF-FE it is identified that the received power is better when incorporating the RF-FE. Moreover, this solution is also less demanding with the platform, since it does not require attitude pointing.

Finally, the best case is achieved having the DIR+RF-FE configuration, in which communication is achieved for all SFs and for any elevation with the 915 MHz modules. In the case of the 868 MHz modules communication is not possible for elevations lower than 30°. This last configuration is the one that can provide more channel capacity.

The scintillation tests are performed considering the same BW of 125 kHz, and an SF of 7. The cases studied are the best and worse of the link budget for these modulation parameters. Moreover, two different coding rates are used, $CR = \frac{4}{5}$ and $CR = \frac{4}{6}$, to asses if having more redundancy increases the throughput. These tests analyze the PDR and the tendency of the received power for different S_4, obtaining also the throughput.

The results of the tests show that overall the throughput decreases as ionospheric scintillation severity increases. For the two best cases, the throughput is lower for the $CR = \frac{4}{6}$ case, because there is more redundancy and less payload data can be sent in the same amount of time. In this case, having more redundancy does not have a positive impact since there is margin in the link budget and not many errors can be detected and corrected.

Comparing the two worse cases, it can be seen that for low values of S_4 having a higher redundancy provides a higher throughput, since the CR is able to correct some of the errors induced in the packets due to the fadings. Although, for more severe scintillation the behaviour is the opposite, since the CR is no longer able to correct these errors, and having larger packets increases the probability of being affected by fadings. Thus, adding more redundancy is only positive in a scenario where the communications are in the limit of the link budget and the scintillation has low or medium severity.

This study has presented the performance of the LoRa technology in satellite-to-ground communications. Nevertheless, this kind of technology enables to establish links with large ranges, paying for a low data rate. Its application in satellite-to-satellite communications may be investigated in future researches, which could promote the creation of satellite networks, such as the ones presented in Internet of Satellites (IoSat) paradigm [30].

Finally, this research was possible thanks to the FI-2019 grant from AGAUR-Generalitat de Catalunya.

REFERENCES

[1] *IEEE Standard for Low-Rate Wireless Networks*, IEEE Standard 802.15.4-2015. Accessed: Nov. 2019. [Online]. Available: https://standards.ieee.org/standard/802_15_4-2015.html

[2] Bluetooth. *Core Specifications*. Accessed: Mar. 2020. [Online]. Available: https://www.bluetooth.com/specifications/bluetooth-core-specification/

[3] Zigbee Alliance. *Zigbee*. Accessed: Mar. 2020. [Online]. Available: https://zigbeealliance.org/solution/zigbee/

[4] K. Mekki, E. Bajic, F. Chaxel, and F. Meyer, "A comparative study of LPWAN technologies for large-scale IoT deployment," *ICT Express*, vol. 5, no. 1, pp. 1–7, Mar. 2019. [Online]. Available: http://www.sciencedirect.com/science/article/pii/S2405959517302953

[5] Z. Qu, G. Zhang, H. Cao, and J. Xie, "LEO satellite constellation for Internet of Things," *IEEE Access*, vol. 5, pp. 18391–18401, 2017.

[6] CubeSat. *Cubesat*. Accessed: Nov. 2019. [Online]. Available: http://www.cubesat.org/

[7] J. Aarons, "Global morphology of ionospheric scintillations," *Proc. IEEE*, vol. 70, no. 4, pp. 360–378, 1982.

[8] Lacuna Space. *Lacuna*. Accessed: Nov. 2019. [Online]. Available: https://www.lacuna.space/

[9] FOSSA Systems. *Fossa*. Accessed: Nov. 2019. [Online]. Available: https://fossa.systems/es/home-spanish/

[10] M. R. Palattella and N. Accettura, "Enabling Internet of everything everywhere: LPWAN with satellite backhaul," in *Proc. Global Inf. Infrastruct. Netw. Symp. (GIIS)*, Oct. 2018, pp. 1–5.

[11] T. Wu, D. Qu, and G. Zhang, "Research on LoRa adaptability in the LEO satellites Internet of Things," in *Proc. 15th Int. Wireless Commun. Mobile Comput. Conf. (IWCMC)*, Jun. 2019, pp. 131–135.

[12] A. A. Doroshkin, A. M. Zadorozhny, O. N. Kus, V. Y. Prokopyev, and Y. M. Prokopyev, "Experimental study of LoRa modulation immunity to Doppler effect in CubeSat radio communications," *IEEE Access*, vol. 7, pp. 75721–75731, 2019.

[13] Sigfox. *Sigfox: The Global Communicator Service Provider*. Accessed: Nov. 2019. [Online]. Available: https://www.sigfox.com/en

[14] 3GPP. *Release 13*. Accessed: Nov. 2019. [Online]. Available: https://www.3gpp.org/release-13

[15] LoRa Alliance. *LoRa Alliance*. Accessed: Nov. 2019. [Online]. Available: https://lora-alliance.org/

[16] Sigfox. *Sigfox Device Radio Specifications*. Accessed: Jun. 2020. [Online]. Available: https://build.sigfox.com/sigfox-device-radio-specifications

[17] A. Guidotti, A. Vanelli-Coralli, M. Caus, J. Bas, G. Colavolpe, T. Foggi, S. Cioni, A. Modenini, and D. Tarchi, "Satellite-enabled LTE systems in LEO constellations," in *Proc. IEEE Int. Conf. Commun. Workshops (ICC Workshops)*, May 2017, pp. 876–881.

[18] Satelliteprome. *Sateliot to Invest USD 5.1m in R&D for Nanosat Constellation*. Accessed: Jun. 2020. [Online]. Available: https://satelliteprome.com/news/sateliot-to-invest-usd-5-1m-in-rd-for-nanosat-constellation/

[19] The Things Network. *Lora World Record Broken: 832km/517mi Using 25 mw*. Accessed: Nov. 2019. [Online]. Available: https://www.thethingsnetwork.org/article/lorawan-world-record-broken-twice-in-single-experiment-1

[20] Lacuna Space. *Lacuna Space Achieves Major Milestone for LoRa in Space*. Accessed: Jun. 2020. [Online]. Available: https://lacuna.space/lacuna-space-achieves-major-milestone-for-lora-in-space/

[21] Dataverse. *Pocketqube Standard*. Accessed: Jun. 2020. [Online]. Available: https://dataverse.nl/api/access/datafile/11680

[22] Fossa Systems. *LoRa Ground Station Development Kit*. Accessed: Mar. 2020. [Online]. Available: https://fossa.systems/product/lora-ground-station-development-kit/

[23] *SX1261/2 Data Sheet DS.SX1261-2.W.APP*, Semtech, Camarillo, CA, USA, 11, rev. 1.1.

[24] Qorvo. *RF5110G*. Accessed: Jun. 2020. [Online]. Available: https://www.qorvo.com/products/p/RF5110G

[25] Skyworks. *Sky67150-396lf: 300 to 2200 MHz Ultra Low-Noise Amplifier*. Accessed: Jun. 2020. [Online]. Available: https://www.skyworksinc.com/-/media/SkyWorks/Documents/Products/1901-2000/SKY67150_396LF_202922I.pdf

[26] E. G. Njoku and E. K. Smith, "Microwave antenna temperature of the Earth from geostationary orbit," *Radio Sci.*, vol. 20, no. 3, pp. 591–599, May 1985.

[27] T. E. Humphreys, M. L. Psiaki, and P. M. Kintner, "Modeling the effects of ionospheric scintillation on GPS carrier phase tracking," *IEEE Trans. Aerosp. Electron. Syst.*, vol. 46, no. 4, pp. 1624–1637, Oct. 2010.

[28] A. Camps, J. Barbosa, M. Juan, E. Blanch, D. Altadill, G. Gonzalez, G. Vazquez, J. Riba, and R. Orus, "Improved modelling of ionospheric disturbances for remote sensing and navigation," in *Proc. IEEE Int. Geosci. Remote Sens. Symp. (IGARSS)*, Jul. 2017, pp. 2682–2685.

[29] J. A. Ruiz-De-Azua, A. Camps, and A. C. Auge, "Benefits of using mobile ad-hoc network protocols in federated satellite systems for polar satellite missions," *IEEE Access*, vol. 6, pp. 56356–56367, 2018.

[30] J. A. Ruiz-de-Azúa, A. Calveras, and A. Camps, "Internet of satellites (IoSat): Analysis of network models and routing protocol requirements," *IEEE Access*, vol. 6, pp. 20390–20411, 2018.

LARA FERNANDEZ (Student Member, IEEE) was born in Barcelona, Spain. She received the degree and M.Sc. degree in telecommunications engineering from the Universitat Politècnica de Catalunya, Barcelona, in 2017 and 2019, respectively, where she is currently pursuing the Ph.D. degree. She is also participating in the *Fly Your Satellite* program from ESA. She is a member of the FSSCat Project, which is the winner of the ESA Sentinel Small Sat (S^3) Challenge of the Copernicus Masters Competition. Her research interests include the Internet of Things, 5G networks, satellite networks, communication systems, and antenna design.

JOAN ADRIA RUIZ-DE-AZUA (Member, IEEE) was born in Barcelona, Spain. He received the degree in aerospace engineering from Supaero, Toulouse, France, in 2015, the degree in telecommunications engineering from the Unversitat Politècnica de Catalunya, Barcelona, Spain, in 2015, and the M.S. degree in network protocols from Supaero, in 2015. He is currently pursuing the Ph.D. degree with the Universitat Politècnica de Catalunya, Barcelona, Spain. He was awarded with the best M.S. thesis on Critical Communications from the Official Spanish Telecommunications Chartered Institute, in 2016. He has participated in different projects of ground segment for Ariane 5 and Ariane 6 programs in GTD company, in collaboration CNES and ESA. He is currently participating in the Fly Your Satellite program from the ESA. He is a member of the FSSCat project, which is the winner of the ESA Sentinel Small Sat (S^3) Challenge of the Copernicus Masters Competition. His research interests include satellite architectures, satellite networks, cognitive networks, the Internet of Things, and embedded software.

ANNA CALVERAS was born in Barcelona, Spain, in 1969. She received the Ph.D. degree in telecommunications engineering from the Universitat Politècnica de Catalunya, Spain, in 2000. She is currently an Associate Professor with the Wireless Networks Group (WNG), Computer Networks Department, Universitat Politècnica de Catalunya. She has been involved in several national and international research or technology transfer projects. She has published in international and national conferences and journals. Her research interests and expertise areas comprise the design, evaluation and optimization of communication protocols and architectures for cellular, wireless multihop networks, ad-hoc networks, wireless sensor networks, the Internet of Things, and application domains, such as smart cities, building automation, and emergency environments.

ADRIANO CAMPS (Fellow, IEEE) was born in Barcelona, Spain, in 1969. He received the degree and Ph.D. degree in telecommunications engineering from the Universitat Politècnica de Catalunya (UPC), Barcelona, in 1992 and 1996, respectively. From 1991 to 1992, he was with the ENS des Télécommunications de Bretagne, France, with an Erasmus Fellowship. Since 1993, he has been with the Electromagnetics and Photonics Engineering Group, Department of Signal Theory and Communications, UPC, where he was an Assistant Professor and an Associate Professor, in 1997. Since 2007, he has been a Full Professor with UPC. He has published more than 215 journal articles in peer-reviewed journals, and more than 420 international conference presentations. He holds 12 patents. His research interests include microwave remote sensing, with special emphasis in microwave interferometric radiometry by aperture synthesis (ESA's SMOS mission), passive microwave remote sensing using signals of opportunity (GNSS- Reflectometry), and use of nano-satellites as cost-effective platforms to test innovative concepts for Earth Observation, such as the 3Cat-2, a 6U-class CubeSat mission launched in August 2016 carrying on-board an innovative GNSS-R payload.